Surface & Coatings Technology 463 (2023) 129538

Contents lists available at ScienceDirect

Surface & Coatings Technology

journal homepage: www.elsevier.com/locate/surfcoat

Study of the flexural behaviour and bonding strength of WC-Co metal matrix composite coatings produced by Laser Directed Energy Deposition

Marta Ostolaza *, Jon Iñaki Arrizubieta, Aitzol Lamikiz, Eneko Ukar

Department of Mechanical Engineering, University of the Basque Country UPV/EHU, Plaza Torres Quevedo 1, 48013 Bilbao, Spain

ARTICLE INFO

Keywords:
Metal Matrix Composites
Laser Directed Energy Deposition
Flexural strength
Wear resistance
Durability

ABSTRACT

Surface coatings enable more durable and sustainable solutions to face the degradation of the functional surfaces of high-added-value components. Particularly, metal matrix composites (MMC) are known to mitigate friction efficiently. However, the bonding strength of MMCs severely limits their durability. Hence, it is not sufficient to focus on wear performance. In this work, the flexural strength and interfacial bonding of Stellite 6/WC MMCs produced by Laser Directed Energy Deposition were investigated. The manufactured coatings exhibited a strong bond to the substrate regardless of the WC content, as no delamination was observed. Additionally, all MMC coatings produced under different processing conditions and with the same composition showed similar elastoplastic behaviour, while specimens containing a higher WC% failed prematurely. This was ascribed to the local embrittlement of the reaction layer surrounding the WC particles, which were found to be crack initiation sites.

1. Introduction

Wear is the main responsible for the damage of high-added-value components in applications that deal with aggressive environments [1]. Additionally, in-service energy losses increase as a result of the operation in non-optimal conditions [2]. Consequently, the industry is pushing for more durable and sustainable solutions to face the surface degradation of critical parts [3]. As opposed to the development of new alloys to improve the surface behaviour of the whole part, surface modification techniques emerge as a flexible alternative [4], where the bulk properties of the base materials are not compromised [5].

The deposition of coatings is a widely extended solution to improve the performance of components under severe environments [6]. Coated surfaces exhibit improved mechanical, thermal, or tribological performance [7]. Typically, a hard phase coating is deposited onto the soft surface and its wear resistance is thereby enhanced [8]. Laser Directed Energy Deposition (L-DED) has gained popularity as opposed to conventional coating techniques [9]. The localised heat input of L-DED prevents the deterioration of the base material, which suffers minimum distortion and heat affection. Moreover, the high cooling rates inherent to L-DED result in finer microstructures and enhanced mechanical properties [6]. Still, a metallurgical bond between substrate and coating is ensured, which is beneficial in terms of flexural resistance and prevents the delamination of the coating [8].

With respect to materials, there is an increasing demand for novel materials which can operate under extreme environments [10]. Hence, powder L-DED is being uplifted as a result of its increased material-wise design freedom [11]. By implementing L-DED systems with multiple hoppers, the composition of the feedstock can be modified in situ [5]. This feature unlocks the processing of advanced materials such as high entropy alloys (HEA), functionally graded materials (FGM), or metal matrix composites (MMCs) [12]. Particularly, surface modification and properties enhancement is the main application of ceramic-reinforced MMCs [13].

MMCs yield unique material properties, e.g. high strength-to-weight ratio and high hardness while retaining the good toughness and ductility of the metal matrix [13]. When an external load is applied to the composite, the load is efficiently transferred from the metal matrix to the stiffer ceramic reinforcement [14]. In addition, the ceramic reinforcements act as barriers to dislocations and oppose plastic deformation. Thus, they prevent the metallic phase from wearing out [15]. Consequently, MMCs also possess a higher wear resistance over monolithic alloys [16]. They are of particular interest in those applications where conventional alloys lack sufficient hardness and wear resistance [17]. For instance, the aerospace industry or the mining and mineral industry could benefit from this solution, considering that wear, erosion,

* Corresponding author.
E-mail addresses: marta.ostolaza@ehu.eus (M. Ostolaza), joninaki.arrizubieta@ehu.eus (J.I. Arrizubieta), aitzol.lamikiz@ehu.eus (A. Lamikiz), eneko.ukar@ehu.eus (E. Ukar).

https://doi.org/10.1016/j.surfcoat.2023.129538
Received 21 February 2023; Received in revised form 12 April 2023; Accepted 13 April 2023
Available online 17 April 2023

and corrosion, are the main mechanisms responsible for the failure of components [18].

So far, several authors described the wear behaviour of MMCs manufactured by means of L-DED. Li et al. investigated the wear resistance of Fe-base and $(Cr,W)_{23}C_6$-WC reinforced coatings. An enhancement of the wear resistance of ceramic-reinforced coatings was observed, and they found an optimal coating composition that would maximise the surface properties [19]. Xie et al. studied the wear resistance of WC-reinforced Co-base MMCs and observed a gradual increase in the wear resistance as a function of the WC content [20]. Similar behaviour was observed by Zhao et al. for WC-reinforced Fe-base [21] and Ni-base [22] coatings. Results showed a significant gain in wear resistance with increasing reinforcement phase. They ascribed this improvement to both the dispersed precipitation of carbides in the matrix and the retained WC particles. Muvvala et al. investigated in greater detail the contribution of the reinforcement particles to wear resistance. They concluded that an excessive decomposition of the reinforcement particles could lead to the embrittlement of the metal matrix. This phenomenon promoted fracturing and spalling of the surface, resulting in a higher wear rate [23]. These works demonstrate that the wear behaviour of MMC coatings improves with increasing reinforcement content, as long as the particle fracture is prevented and no third body wear mechanism occurs [16]. Typically, the ceramic particles control the plastic flow of the metal matrix and the main wear mechanism will transform from severe adhesive to mild adhesive-abrasive wear with increasing reinforcement content [24].

Whilst there has been a strong focus on the wear behaviour of MMC coatings; little research has been carried out on the mechanical properties related to strain and flexural behaviour. However, the flexural strength and the substrate-coating interfacial strength are key aspects which enable their safe and durable in-service operation [7]. On the other hand, the surface properties and mechanical behaviour of MMCs depend strongly on the interfacial bonding between macro constituents. So has been stated by several researchers [25,26]. In ceramic-reinforced MMCs produced by L-DED, complex hierarchical microstructures are generated. Partial dissolution of the reinforcement phase takes place, which originates interfacial reactions between ceramics and metals [27]. On the one hand, the reaction layer ensures cohesion and proper load transfer between macro constituents [26]. Conversely, the metal-ceramic reaction may cause the embrittlement of the metal matrix, which is detrimental to the mechanical properties of the composites [28]. Previous authors studied the microstructural phases present in MMC coatings from a crystallographic and compositional perspective [29–31]. In any case, a balance in the interfacial reaction must be sought. The bond should guarantee an efficient load transfer from the matrix to the reinforcement while preserving the good flexural behaviour of the coatings. This matter can be addressed by either controlling the process parameters and tuning the thermal cycle during the deposition process [18,32] or by limiting the ceramic content of MMC coatings [33].

Summing up the state-of-the-art outlined above, it is apparent that wear testing is not sufficient to enable the production of high-quality MMCs coatings. Indeed, the flexural behaviour needs to be further tested and the understanding of the failure mechanisms improved. Hence, based on the existing literature, the novelty and contributions present in this research are to:

i. Investigate the influence of the process parameters and the thermal cycle on the surface hardness of MMC coatings.
ii. Investigate the influence of the process parameters and the thermal cycle on the flexural strength of MMC coatings.
iii. Correlate the gain obtained in terms of wear to the extent of the loss in flexural properties in MMC coatings produced with different WC%.
iv. Understand the key aspects of the performance and failure mechanisms of MMC coatings.

To that end, WC-reinforced Co-base MMC coatings have been produced in the present work. During the deposition process, the melt pool and substrate temperatures were monitored. Then, the surface hardness of the manufactured specimens was analysed and correlated with microstructural aspects. Later, the flexural strength of the specimens was estimated based on the standard 3-point bending test. Lastly, the wear resistance of the specimens was studied through ball-on-disc dry sliding tests.

2. Materials and methods

2.1. Materials

AISI H13 hot-work tool steel plates with dimensions 45 × 35 × 8 mm^3 were used as substrates for the specimens built for hardness and flexural testing purposes. AISI H13 is widely employed for the production of tooling and industry components, which is an eligible application for this kind of MMC coatings. Conversely, AISI 1045 carbon steel plates with dimensions 70 × 70 × 14 mm^3 were used as substrates for wear testing specimens. Indeed, given the thickness of the coatings produced, the influence of the substrate material on the tribological testing should be negligible, and the widespread availability of AISI 1045 makes it an efficient substrate alternative. The MMC coatings consisted of a Co-base alloy similar to Stellite 6 (MetcoClad 6) and WC reinforcement particles (MetcoClad 52001). The mixed powder feedstock was delivered through a discrete coaxial nozzle. The particle size distribution of the feedstock powders is provided in Table 1 and their composition is shown in Table 2.

2.2. Specimen production by means of L-DED

The specimens were produced in a TruLaser Cell 3000 L-DED machine. The system features a Yb:YAG disk laser with a 1030 nm wavelength and 3 kW maximum output power. During all experiments, the laser spot diameter at the focal plane was set at 1.75 mm and measured with a coaxial CCD (charge-coupled device) camera. Similarly, the volumetric rate of the feedstock was fixed at 0.35 cm^3/min. The coating specimens consisted of two layers, which were deposited following a zig path with a 30 % overlap between adjacent clads. The total thickness of the MMC specimens was approximately 1 mm and the dilution, roughly, 175 μm. The coating distribution in the substrate and detailed dimensions of the deposits are depicted in Fig. 1. The first image, Fig. 1(a), corresponds to the specimens produced for surface hardness characterisation and 3-point bending tests; whereas the second image, Fig. 1(b), corresponds to the specimens produced for wear testing.

During the L-DED process, the thermal cycle was monitored through a 2-colour IMPAC pyrometer (IGAR 12-LO LumaSense Technologies), which was focused on the centre of the MMC specimen during the deposition of the first layer, as this is the layer where the bonding with the substrate is developed. The employed pyrometer has a 60 Hz acquisition frequency and a 550–2500 °C measuring temperature range. In addition, the temperature of the substrate was monitored by means of a type K thermocouple. The acquisition rate was 1 Hz and the maximum

Table 1
Particle size distribution of the feedstock powders.

Diameter (μm)	Mass fraction (−)	
	MetcoClad 6	MetcoClad 52001
d < 45 μm	0.3	3.2
d > 45 μm	99.7	96.8
d > 75 μm	48.8	47.8
d > 106 μm	2.5	4.77
d > 125 μm	0.0	0.34
d > 150 μm	0.0	0.0

Data from Oerlikon Metco datasheets for MetcoClad 6 and MetcoClad 52001.

Table 2
Composition of the materials employed %wt.

Material	Co	Cr	W	Fe	Ni	Si	C	Mo	Mn	P	S	V
MetcoClad 6	Bal.	28.0	4.0	3.0	3.0	1.5	1.0	1.0	0.0	0.0	0.0	0.0
MetcoClad 52001	0.0	0.0	Bal.	0.19	0.0	0.0	4.03	0.0	0.0	0.0	0.0	0.0
AISI H13	0.0	5.13	0.0	Bal.	0.0	1.03	0.39	1.43	0.4	0.03	0.03	1.0
AISI 1045	0.0	0.0	0.0	Bal.	0.0	0.0	0.43–0.50	0.0	0.6–0.9	0.04	0.05	0.0

Data from ASTM A681-08 Standard Specification for Tool Steels Alloy, ASTM A29M-16 Standard Specification for General Requirements for Steel Bards, Carbon and Alloy, Hot-Wrought, and Oerlikon Metco datasheets for MetcoClad 6 and MetcoClad 52001.

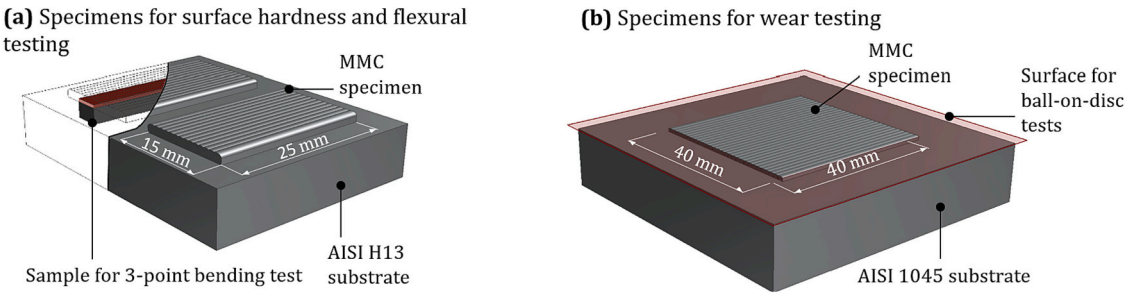

Fig. 1. Dimensions of MMC specimens produced for the corresponding analysis and regions of interest: (a) specimens for surface hardness measurement and flexural testing and (b) specimens for wear testing.

admissible temperature was 1300 °C, which is enough considering that the measuring point is not located close to the area melted by the laser. Lastly, the thermal field of the specimens was recorded by means of an Optris PI thermal camera. The images of the IR (infrared) camera were used for a global analysis of the thermal field during the deposition process. However, due to emissivity variations of the different materials and temperature gradients, the acquired videos were used strictly for a qualitative comparison.

The primary focus of the present work is to investigate the effect of the process parameters and composition of the feedstock on the flexural strength of MMC coatings deposited by L-DED. On the one hand, the mechanical properties of composite materials are dominated by the interfacial reactions between the reinforcement and matrix phases. The interaction between macro-constituents depends on the thermal cycle of the L-DED process, namely, on the melt pool lifetime. Thus, experiments with different feed rates have been produced. On the other hand, additional experiments with varying preheating temperatures have been carried out. The preheating system employed consists of an induction hob. For safety reasons, the system was switched off during the L-DED process.

Specimens containing 5 % WC and 10 % WC were produced to avoid the excessive dissolution of the reinforcement phase. Indeed, a controlled decomposition of the WC particles alleviates the embrittlement of the matrix [33], which according to previous authors is beneficial for the tribological behaviour [19,23]. Moreover, a minimum variation of 5 % WC is rendered necessary to appreciate relevant variations in the final behaviour of the coating and thus, to draw significant conclusions. In Table 3, the designed experiments are summarized.

Table 3
Process parameters employed in specimens for surface hardness and flexural testing.

Specimen	Power, P (W)	WC content, (%)	Feed rate, v_F ($mm \cdot min^{-1}$)	Preheating temperature, T_{in} (°C)
A0	700	5	300	Room temperature
A1			350	Room temperature
A2			400	Room temperature
B1			400	225
C0	700	10	300	Room temperature
C1			350	Room temperature
C2			400	Room temperature
D1			400	225

2.3. Microstructural characterisation, surface hardness, and flexural resistance

The deposited specimens were post-processed for further analysis. Longitudinal sections were extracted through wire Electro Discharge Machining (w-EDM) for microstructural analysis. The metallographic samples were mounted, ground, and polished following the appropriate metallographic procedure. The microstructure was revealed through electrolytic etching with 10 % oxalic acid solution at 10 V for 1–3 s and a Nikon Optiphot-100 microscope was employed for microstructural inspection.

In order to quantify the sub-grain dendritic scale, the secondary dendrite arm spacing (SDAS) was measured following the methodology proposed in [34], as shown in Fig. 2. For each sample, 25 discrete measurements were performed, in different regions located at the top layer of the samples. Additionally, high magnification images and Energy-dispersive X-ray spectroscopy (EDX) measurements were carried out through the JEOL JSM-6400 scanning electron microscope (SEM).

The hardness of the surface was characterised in compliance with the ISO standards for the Rockwell C hardness test (ISO 6508-1:2016). The surface of the deposited specimens was machined through w-EDM and manually ground with SiC papers. The Computest SCX portable electronic hardness tester was employed and 10 indentations were carried out in each specimen. The indentations were randomly distributed throughout the surface of the specimen but spaced at least 2 mm. A

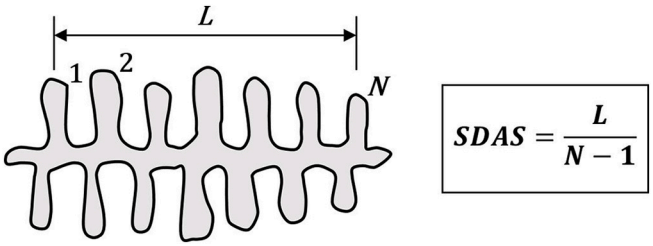

Fig. 2. Measurement of the secondary dendrite arm spacing (SDAS).

preload of 98.07 N and a load of 1471 N were employed, in compliance with the standards.

Two samples for 3-point bending tests were extracted from each specimen through w-EDM, as shown in Fig. 1(a). Firstly, about 200 μm were removed from the surface of the L-DED samples to obtain a 800 μm-thick coating. Then, the test samples were cut through EDM to the final dimension of 20 × 4 × 2.6 mm^3. Actual images of the produced specimens and a metallographic image of the longitudinal section are shown in Fig. 3.

The flexural behaviour of the MMC coatings was analysed through 3-point bending tests. In addition, two AISI H13 samples with dimensions 20 × 4 × 2.6 mm^3 were also tested to characterise the behaviour of the substrate material. The flexural tests were carried out in an INSTRON 8801 testing machine at room temperature and a constant cross-head speed of 1 $mm{\cdot}min^{-1}$. In Fig. 4, a schematic description of the tests and samples employed is provided.

During the 3-point bending test, the displacement of the crosshead and the load were monitored. Additionally, the tests were recorded with a high-speed camera to observe the failure mechanism of the coatings. After failure, the samples were examined by means of the JEOL JSM-6400 scanning electron microscope.

2.4. Wear testing

The wear resistance of the surface coatings was assessed through the ball-on-disc dry sliding method. The target surface shown in Fig. 1(b) was machined by means of w-EDM to eliminate the waviness of the overlapped clads and to attain the desired 800 μm thickness of the coating. Then, test surfaces were ground with SiC abrasive papers to remove any traces of the w-EDM and to ensure a Ra < 1 μm. Lastly, they were washed in acetone.

Experiments were carried out in a Microtest MT tribometer at room temperature. A 6 mm diameter WC94/Co6 mirror-like spherical pin was contacted at 12.5 mm from the centre of the disc. The disc rotated at 324 rpm and a 20 N load was applied. The total distance tested was 833.33 m.

The frictional behaviour of the coating was evaluated through the average CoF (Coefficient of Friction) in the stable regime. Also, the wear resistance of the coatings was measured according to the area of the groove. The worn track was examined through a Leica DCM3D confocal microscope. Surface topographies of four regions of the groove were obtained, at the angular positions of 0°, 90°, 180°, and 270°. Then, profiles of the cross-section of the groove were extracted and the area corresponding to the worn material was calculated. Lastly, the worn surface was inspected at the JEOL JSM-6400 scanning electron microscope.

3. Results and discussion

In this section, the results obtained during the experiments are summarized and discussed. The thermal cycle recorded during the deposition process and the properties of the MMC coatings are assessed; namely, the microstructure, surface hardness, flexural strength, and wear resistance.

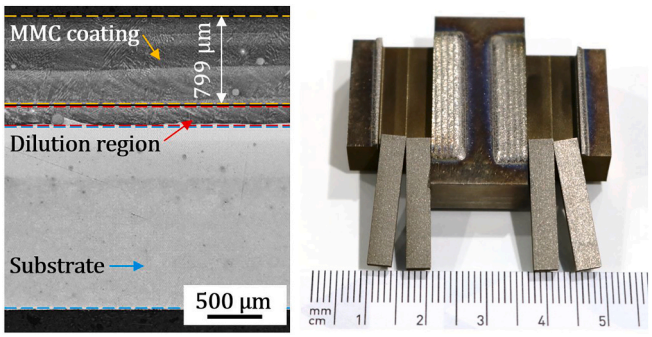

Fig. 3. Metallography of the tested coating and actual images of the samples employed for 3-point bending tests.

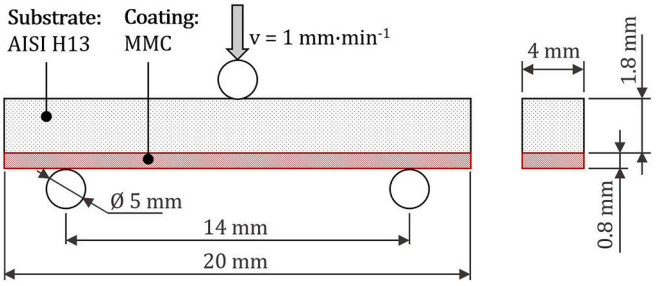

Fig. 4. Schematic diagram of the 3-point bending tests and sample dimensions.

3.1. Thermal analysis of the L-DED process

In terms of thermal analysis, no significant variations were observed for specimens containing 5 % and 10 % WC. For the sake of clarity, only data corresponding to 5 % WC coatings are reported and discussed.

Firstly, results concerning the temperature of the substrate during the deposition process are addressed. In Fig. 5, the thermal history recorded by the thermocouple is shown. Manufacturing cycles corresponding to preheated and not preheated specimens produced at 400 $mm{\cdot}min^{-1}$ are reported. Note that the sensor was located on the periphery of the substrate.

The instant when the preheating system is turned off and when the L-DED process starts can be clearly identified in Fig. 5. The temperature drop at the core of the substrate will be much lower as compared to that measured by the thermocouple. The heat dissipation at the surfaces and, especially, at the periphery of the substrate is more prominent. Nonetheless, the obtained data is useful to establish a comparison between specimens produced at room temperature and those that were preheated. Preheated specimens maintain a higher temperature of the substrate during the entire deposition process: the average temperature of the substrate during the deposition of the first layer was 61 °C and 133 °C, for the room temperature (A2) and preheated (B1) experiments, respectively.

Secondly, the lifetime of the melt pool (Δt_{liq}) and the cooling rate of the L-DED process (C) were calculated based on the data acquired by the pyrometer. Δt_{liq} corresponds to the period of time during which the temperature of the material is over the liquidus temperature (T_{liq}). In turn, the solidification cooling rate was calculated based on the thermal gradient between the solidus and the liquidus temperatures [35] and

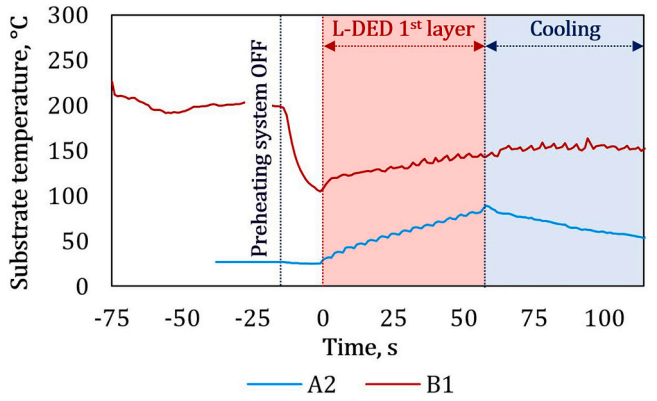

Fig. 5. Thermal history at the periphery of the substrate for specimens A2 (not preheated) and B1 (preheated) measured by the K-type thermocouple.

according to (Eq. (1)). The thermal properties of the metal matrix, that is, MetcoClad 6 were used for such calculations. Hence, a liquidus temperature (T_{liq}) of 1360 °C and a solidus temperature (T_{sol}) of 1260 °C were considered according to [36]. On the other hand, t_{Tsol} and t_{Tliq} correspond to the time instants where the solidus and liquidus temperatures are reached during solidification, respectively.

$$C = -\frac{T_{liq} - T_{sol}}{t_{Tliq} - t_{Tsol}} \quad (1)$$

Fig. 6 shows the calculated cooling rate, melt pool lifetime, and the maximum melt pool temperature. The melt pool lifetime decreases with increasing feed rate (A0 → A2) and so does the maximum melt pool temperature, whilst the opposing trend is observed for the cooling rate. Similarly, the preheated specimen (B1) exhibits a longer melt pool lifetime and lower cooling rate as compared to the specimen produced at room temperature (A2). The obtained results are in good accordance with the expected trends.

The obtained variation in the thermal history of specimens will affect the microstructure and the subsequent mechanical properties of the MMC coatings. The solidification cooling rate, especially, is strongly correlated to the dendritic scale. At the same time, a finer dendritic scale is known to contribute to Hall-Petch strengthening. These phenomena are further discussed in the following subsections.

The difference of the thermal fields obtained with varying feed rates and preheating temperatures is clearly observed in Fig. 7. When increasing the feed rate from 300 mm·min^{-1} (A0) to 400 mm·min^{-1} (A2), the energy input is reduced and the thermal field is modified accordingly. In the same manner, a substantial change is observed between the preheated specimen (B1) and the specimen manufactured at room temperature (A2).

3.2. Characterisation of the microstructure

Samples manufactured with different processing conditions exhibit different microstructures in terms of microstructural refinement. Additionally, the modification of the process parameters and the thermal history during the L-DED process could also affect the composition of the matrix by promoting the decomposition of the reinforcement phase [33]. Carbides are often in situ synthesised in MMCs due to the decomposition of the reinforcement particles, which is due to the high temperatures present during the L-DED process. However, no such phenomenon was observed, at least, not to a remarkable extent, and the interaction between the ceramic and metallic phases was limited to the surroundings of WC particles.

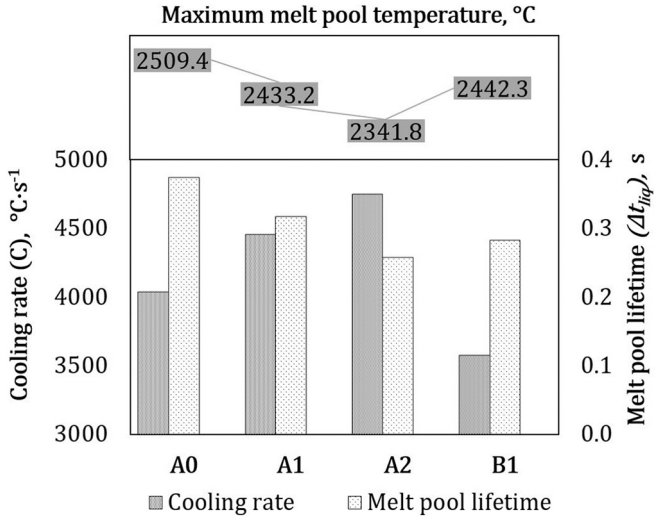

Fig. 6. Cooling rate, melt pool lifetime and maximum temperature of the melt pool of the 5 % WC specimens fabricated with different processing conditions.

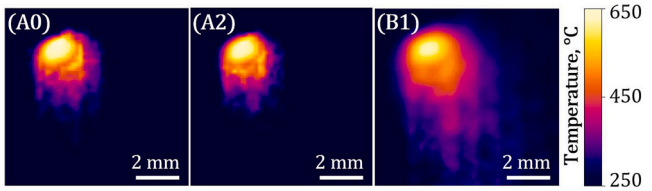

Fig. 7. Thermal field of specimens produced at different feed rates (A0 vs. A2) and preheating temperatures (A2 vs B1), measured by the IR camera.

In Fig. 8, the microstructure of the matrix is shown with a higher magnification. The dendritic and interdendritic phases can be distinguished. In the surroundings of the WC particle, W-rich microstructural phases are generated as a result of the decomposition of the ceramic phase. Nonetheless, due to the low volumetric fraction of tungsten carbide particles and the fast cooling rates during processing, no dispersion of such phases over the matrix has been observed. Moreover, the overall compositional modification of the matrix is negligible and the matrix is just locally affected. This is ascribed to the controlled metal-ceramic interaction.

EDX analyses of the dendritic and interdendritic regions are performed to support the BSE SEM images. Higher W is measured in the interdendritic phase (A), which, according to the literature, is typically composed of eutectic Cr-, Co-, and W-rich carbides [37]. Opposingly, higher Co is measured in the primary dendritic phase (B), which has been characterised as an fcc solid-solution based on Co—Cr by previous authors [37]. This differentiation is clearly illustrated in the EDX maps shown in Fig. 9.

To quantify the dendritic scale resulting from the different processing conditions, the SDAS was measured. In Fig. 10, the SDAS of the samples manufactured at room temperature with respect to the feed rate is plotted. The high standard deviation of the measurements is due to the inhomogeneous cooling inherent to L-DED, which is why several measurements were carried out to guarantee the reliability of the mean values. Despite the dispersion of the experimental data, a clear trend can be observed. Indeed, samples produced at lower feed rates exhibit a higher SDAS, hence a coarser microstructure. This is due to the lower cooling rates associated to these processing conditions (Fig. 6). Also, samples with higher WC content exhibit a slightly finer microstructure, which could be ascribed to the refining effect of embedded carbides in

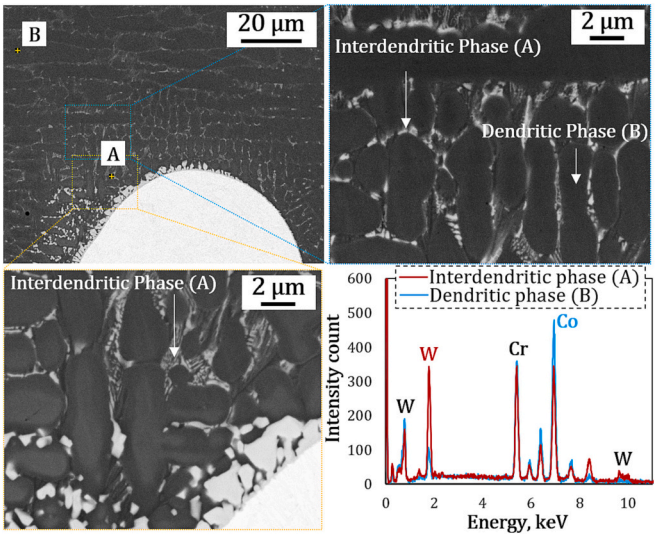

Fig. 8. BSE (backscattered electrons) SEM micrographs of the microstructure of the matrix and EDX analysis of the interdendritic and dendritic phases (Sample C2).

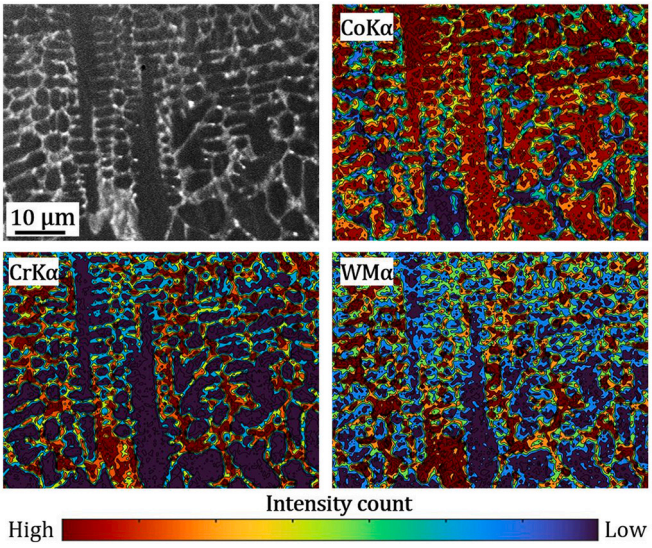

Fig. 9. BSE SEM image and EDX maps of the matrix of sample C2.

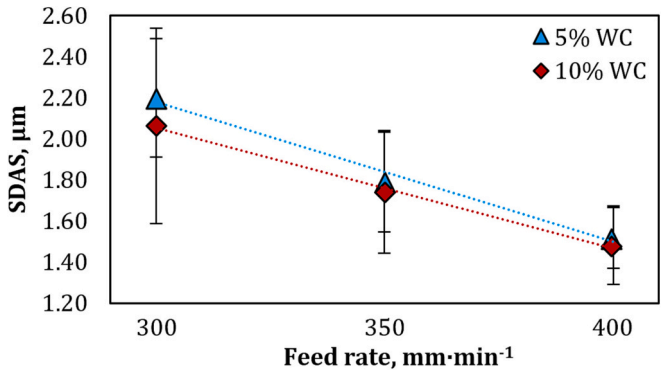

Fig. 10. Secondary dendrite arm spacing (SDAS) of samples produced at room temperature with respect to the feed rate.

the matrix, and the fact that more nucleation points are present. However, in this case, the dispersion of the measurements is too high to extract any clear conclusions.

Due to the higher cooling rate of the coatings produced at 400 mm·min^{-1} (Fig. 11-A2), finer microstructures as compared to the specimens produced at 300 mm·min^{-1} (Fig. 11-A0) are generated.

This effect can be observed both in the top layer and in the solidification structure from the substrate. At higher magnifications, this phenomenon is more evident, and specimens subject to higher cooling rates (Fig. 12-A2) exhibit finer dendrites as compared to those subject to lower cooling rates ((Fig. 12-A0). A similar effect is observed when preheating the substrate prior to the deposition process. Preheating

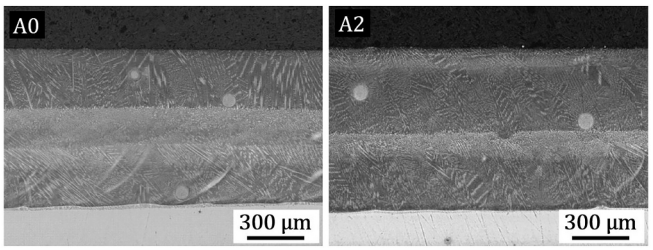

Fig. 11. Longitudinal view of specimens employed for 3-point bending tests. A0 and A2 correspond to coatings produced at 300 mm·min^{-1} and 400 mm·min^{-1}, respectively.

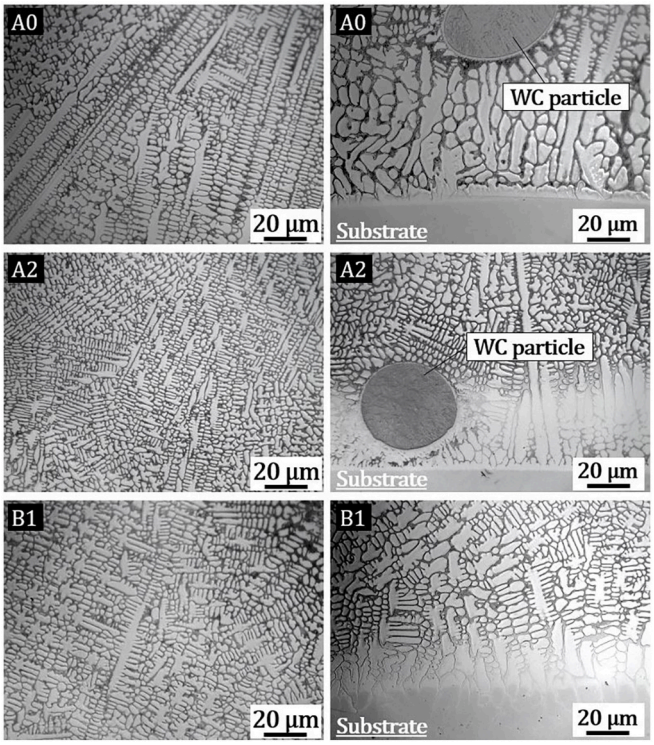

Fig. 12. Microstructure of specimens A0, A2, and B1, manufactured at different feed rates and preheating temperatures. Left-hand images correspond to the top layer of the coating, while right-hand images show the interface between the coating and the substrate.

decreases the cooling rate, as observed in the pyrometry measurements (Fig. 6). Therefore, the microstructure generated during the solidification and cooling process is coarser (Fig. 12-B1).

3.3. Characterisation of the surface hardness

The improvement in surface properties and wear resistance is usually accompanied by an increase in surface hardness. Therefore, in the present work, the hardness of the deposited MMC specimens is investigated at the macroscale level. In this manner, the contribution of the reinforcement particles and the matrix are accounted for. The results obtained are summarized in Fig. 13.

In terms of WC content, an increase in surface hardness with increasing WC% is observed. The correlation is met for all parameters tested. This is due to the contribution of WC to the plastic properties of the MMC. Indeed, ceramic particles act as load-bearing constituents and oppose the plastic deformation of the matrix.

As far as the feed rate is concerned, specimens manufactured at lower feed rates exhibit lower surface hardness. Likewise, the surface hardness decreases for preheated specimens. Once again, these trends are observed for both tested compositions, i.e. 5 % WC and 10 % WC. The obtained results are in good agreement with the thermal and microstructural analysis of the specimens. Samples with finer microstructures present a higher hardness, as suggested by the Hall-Petch correlation. Consequently, the influence of the tungsten carbide particle decomposition on the hardening of the coatings is minor and the variation of the hardness for equal composition coatings is mainly ascribed to the grain refinement attained as a consequence of higher cooling rates.

In Fig. 14, the correlation between the SDAS, the cooling rate during the deposition process, and the hardness of the samples is shown for samples produced at different feed rates with no preheating. Overall, a good agreement is obtained. Indeed, the cooling rate is inversely correlated to the SDAS, while the hardness and the SDAS are directly

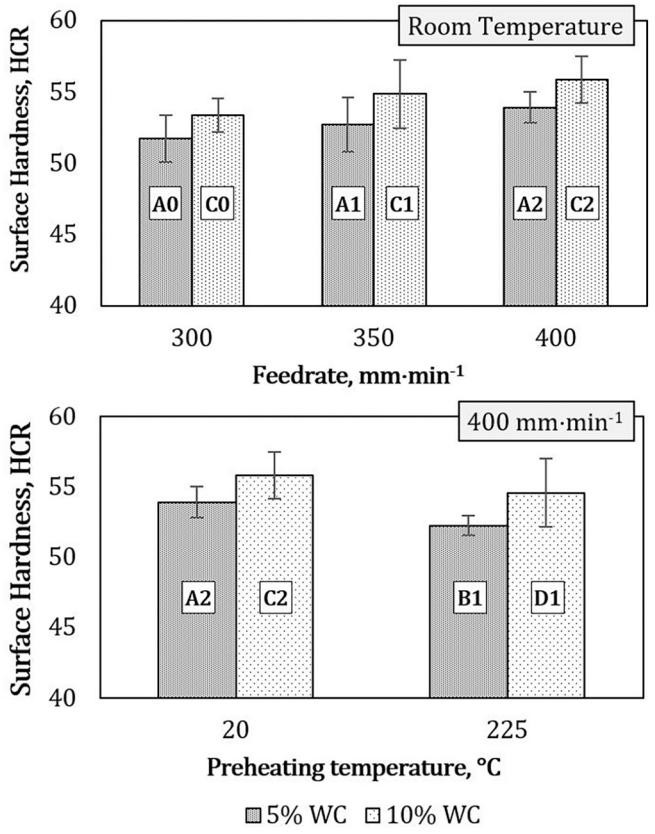

Fig. 13. Surface hardness according to the feed rate and preheating temperatures.

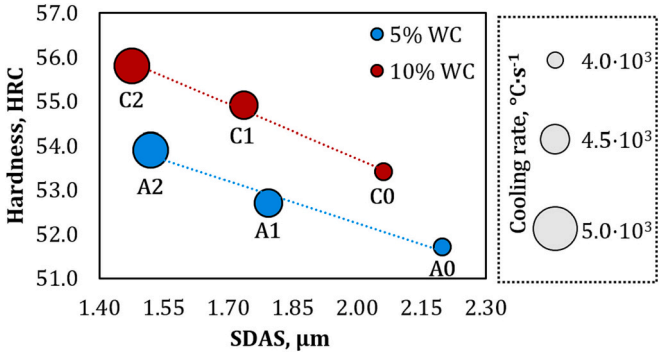

Fig. 14. Surface hardness of MMC composites as a function of the SDAS and the cooling rate of the process.

correlated. As a consequence, it can be inferred that the hardening of the MMC coatings is governed by the grain refinement and the thermal history of the processing, at least in the studied experimental domain. In the same line, samples containing a higher amount of WC (C series) exhibit a higher hardness as compared to the homologously produced A series, which is in good accordance with the expected results. The same trend was observed in the preheated samples.

3.4. Characterisation of the flexural resistance

The durability and in-service operation of a coated component are strictly conditioned by the bond between the substrate and the coating. In the case of MMCs, ensuring a correct load transfer from the matrix to the ceramic particles is also critical, as failure to do so might aggravate the generation of voids in the interface between macro constituents. Hence, in this section, the flexural strength of MMCs manufactured with different parameters is reported.

It is apparent that a sound metallurgical bond is developed between the reinforcement phase and the matrix during the L-DED process (Fig. 15). The high-temperature processing associated with L-DED promotes the partial decomposition of the WC particles and enables the interaction between the matrix and the discrete reinforcement particles. This bond is evidenced by the reaction layer formed around the particles, with a graded composition of the W element (Fig. 16). Hence, a metallurgical bond is attained and a proper load transfer between constituents should occur during the flexural testing.

Test results corresponding to samples A2 and C2, that is, 5 % and 10 % WC manufactured at 400 mm·min^{-1} are gathered in Fig. 17. Additionally, the behaviour of the substrate, AISI H13, is shown as a reference, which exhibits a ductile behaviour. On the contrary, coated samples present a loss in ductility, as their deformation at fracture is considerably lower. Due to the contribution of the metal matrix and improved mechanical properties of the MMC coatings, material plastification occurs at higher loads in coated samples.

In Fig. 17-(1), the instant corresponding to the crack initiation is shown. The crack originates at the surface of the coating, where the highest tensile stress is found. Then, it propagates through the coating and into the substrate (Fig. 17-(2)), meaning that the bond between the coating and the substrate is strong. Otherwise, delamination would have occurred. Such behaviour was observed in all tested samples and no delamination was reported in any specimen.

Coatings with 5 % and 10 % WC show similar elastoplastic behaviour. However, the samples with higher WC% fail at a lower load and deformation (Fig. 17). On the one hand, with an increasing amount of ceramic particles, the probability of WC particles containing flaws increases [38]. On the other hand, the matrix is locally embrittled around the WC ceramic particles, due to the W-rich carbide reaction layer observed in Fig. 16. Moreover, the embedded particles have been reported to provoke stress concentrations, which will further contribute to cracking. Hence, specimens with higher WC% will contain more crack nucleation sites.

In order to account for the relevance of residual stresses and their influence on the failure of coatings, the resulting residual stresses at the surface of the coatings after the deposition process were measured. In this regard, the generation of residual stresses in fusion-based metal AM is currently one of the most challenging issues. This phenomenon rules cracking, local deformation, and warping, which cause premature failure of additively manufactured components.

The surface of sample C2 exhibited a 221.6 ± 50.2 MPa tensile stress after deposition. Preheating has been extensively proposed to mitigate this issue, however, no improvement in the flexural resistance of coated samples was observed with preheating. Therefore, it can be inferred that the variation of the residual stresses resulting from the different processing conditions does not dominate the failure of MMC coatings under flexural loads, most certainly because residual stresses act at a more local scale as compared to flexural testing.

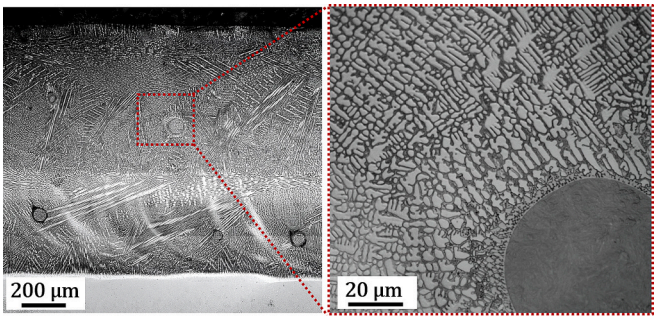

Fig. 15. Metallography of the particle-matrix interface.

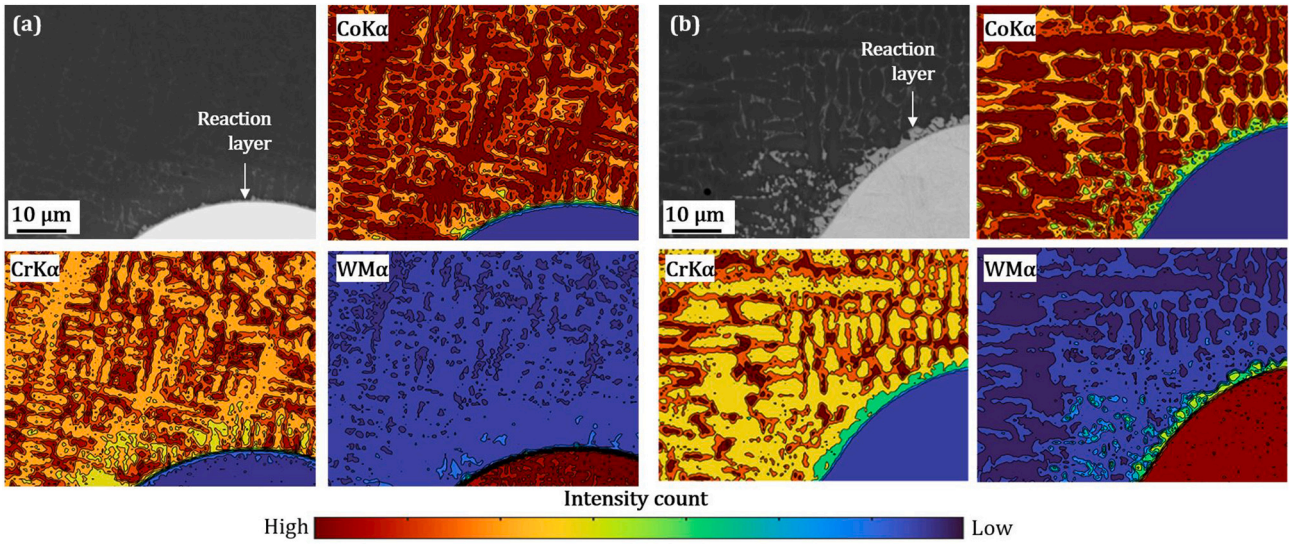

Fig. 16. BSE SEM images and EDX maps of the reaction layer for (a) 5 % WC, sample A2 and (b) 10 % WC, sample C2, both of them produced at 400 mm·min^{-1}.

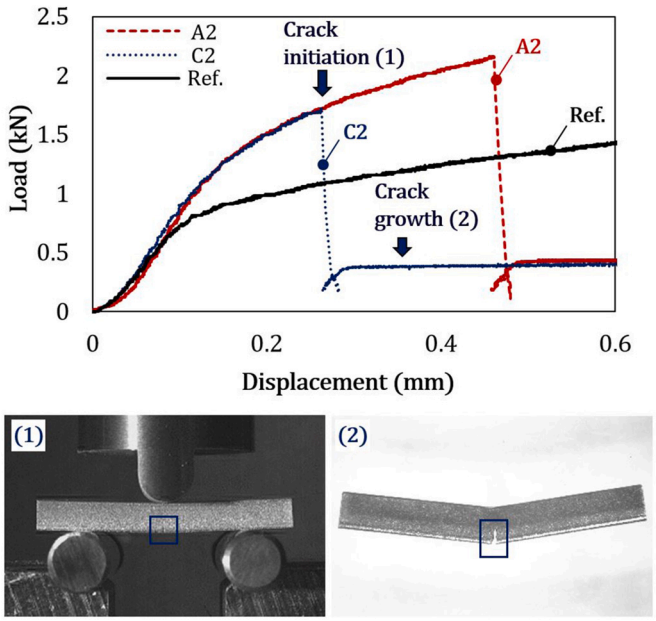

Fig. 17. Load vs. position data corresponding to 3-point bending tests. Sample C2: (1) Instant when crack initiates and (2) Sample after crack propagation through the substrate.

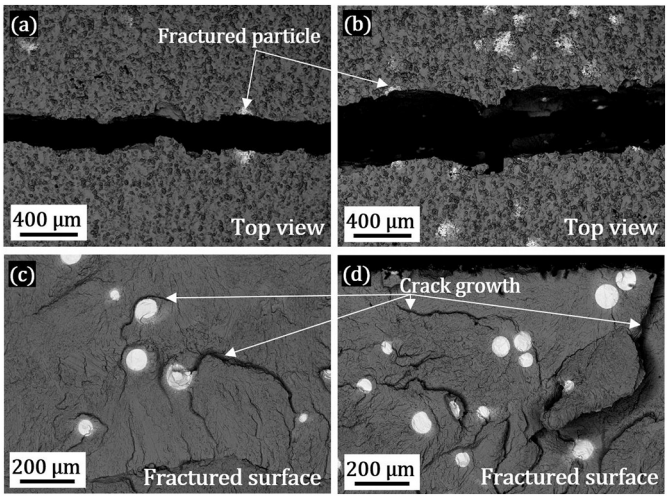

Fig. 18. BSE SEM micrograph of the top view of fractured specimens (a-b) and fractured surfaces (c-d) of specimen A2 (a-c) and C2 (b-d).

In Fig. 18, SEM micrographs of the top view of the fracture and the fractured surface for specimens containing 5 % WC (a-c) and 10 % WC (b-d), are shown. On the one hand, the high-quality bond between the matrix and the particles is confirmed, as cracks propagate across the particles, as opposed to through the particle-matrix interface Fig. 18(a-b). On the other hand, based on the morphology of the fractured surfaces, the failure of the specimens under flexural load is ascribed mainly to nucleation, growth, and coalescence of voids.

The specimen containing 10 % WC (Fig. 18(d)) shows a higher crack density, which explains their premature failure. Ceramic particle agglomeration often occurs in MMCs produced by L-DED. This is partly due to the heterogeneous particle distribution by the nozzle. In addition, their settlement in the matrix is ruled by gravitational and fluid-dynamic phenomena, which are extremely hard to control. Due to the higher amount of WC particles present in the 10 % WC specimen, more particle clusters will be formed. This fact inevitably results in a faster coalescence of cracks and premature failure of the specimens under flexural loads. This phenomenon was evidenced during the SEM inspection of the fractured surfaces, as a higher crack density was observed in regions with particle clusters are found, meaning that the reinforcement particles actively contribute to failure, as they are a preferred site for crack nucleation and growth.

As far as the fracture mechanism is concerned, mixed brittle-ductile mechanisms were observed (Fig. 19). The WC reinforcement particles exhibit a brittle fracture, while the matrix presents a ductile tearing and an interdendritic fracture. However, no significant necking was observed. Ikubanni et al. attributed the low plastic deformation of the matrix to the rapid and intensive nucleation, growth, and coalescence of voids in MMCs [39].

Regarding the influence of the process parameters on the flexural behaviour, no clear conclusions could be drawn. Similar fracture loads and deformations were reported for all samples having the same composition, regardless of the feed rate and the preheating temperature. The results summarised in Table 4 indicate that the influence of the microstructural aspects has a negligible effect on the flexural resistance of MMC-coated specimens. It is concluded that as long as high-quality coatings with no significant defects are produced, this aspect of coated

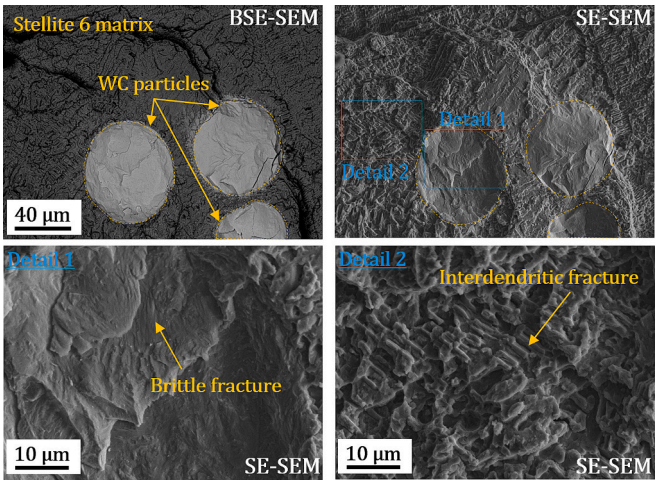

Fig. 19. BSE (backscattered electrons) and SE (secondary electrons) SEM micrographs of the fracture surfacAe of specimen C2, showing the brittle fracture of the reinforcement particles (Detail 1) and interdendritic fracture (Detail 2) of the metal matrix.

Table 4
Summary of results obtained in the 3-point-bending tests.

Specimen	Ultimate load (N)	Deformation at fracture (mm)
A0	2018 ± 18	0.391 ± 0.006
A1	2130 ± 18	0.427 ± 0.009
A2	2141 ± 25	0.458 ± 0.004
B1	2179 ± 79	0.505 ± 0.011
C0	1610 ± 17	0.224 ± 0.008
C1	1547 ± 11	0.212 ± 0.006
C2	1710 ± 25	0.249 ± 0.020
D1	1617 ± 66	0.213 ± 0.007

specimens should not be compromised by the L-DED parameters employed, at least in the experimental domain studied.

Note that the experimental domain was chosen to minimise the decomposition of the WC particles, which would be detrimental to the flexural performance of the MMC coatings. On this basis, the optimisation of the process parameters should focus on other aspects of the coatings, such as maximising the hardness. For the wear testing, specimens showing the highest hardness have been selected for further investigation, namely, A2 and C2.

3.5. Characterisation of the wear resistance

The wear behaviour of 5 % and 10 % WC coatings produced at 400 mm·min^{-1} was evaluated through ball-on-disc dry sliding tests at room temperature. In Fig. 20, surface topographies and cross-sectional profiles corresponding to the worn areas are shown. The wear is much more acute in the coating manufactured with 5 % WC and it can be concluded that a higher volumetric fraction of WC results in a smaller wear scar. In MMC coatings, the tungsten carbide particles prevent the matrix material from wearing off and minimise the material loss during the sliding test.

No traces of fractured WC particles nor particle pull-outs were observed (Fig. 21). In addition, no evidence of third-body wear mechanism was found. Consequently, it can be inferred that the reinforcement phase contributed positively to the wear resistance of the MMC coating. Mild abrasive and adhesive wear mechanisms were observed, which are evidenced by the abrasion grooves and the oxide glaze exhibited in the worn surfaces (Fig. 21). The formation of Cr- and Co-oxides glaze is typical in Co-base alloys subject to frictional loads. The oxide film mitigates wear as it serves as a lubricant in the sliding friction. In addition, the EDX map in Fig. 21 indicates that the oxides adhere to the worn WC particles, further mitigating abrasive wear.

In Fig. 22, the area of the scar and the Coefficient of Friction (CoF) of specimens containing 5 % and 10 % WC are quantitatively compared.

A slight increase in the CoF with increasing WC% is observed, although the area of the worn groove decreases significantly. This could be ascribed to the lubricant effect of the oxide glaze formed. Therefore, it is only logical that surface coatings containing a higher amount of matrix material will have a lower CoF. However, if a closer look is taken at the wearing off of the pin, a significantly larger worn area is exhibited by the pin used in the 10 % WC specimen. Therefore, the increased frictional intensity of the sliding pair in the 10 % WC experiment evidenced by the higher CoF is manifested in the higher wear suffered by the pin (Fig. 23).

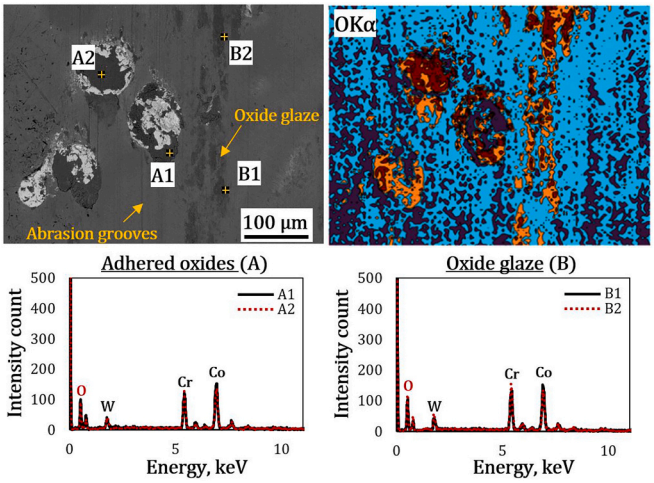

Fig. 21. BSE SEM micrograph of the worn surface of specimen C2. In addition, an EDX map corresponding to the oxygen content and EDX point analyses of adhered oxides and the oxide glaze are shown.

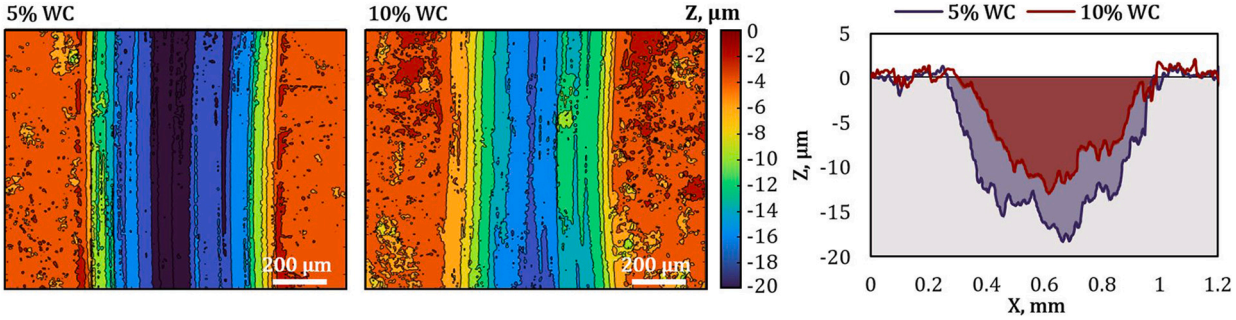

Fig. 20. Surface topographies and cross-sectional profiles of the grooves after ball-on-disc testing.

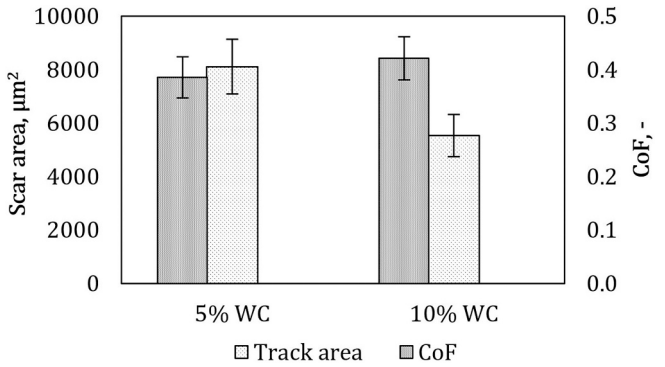

Fig. 22. Area of the scar and CoF of the ball-on-disc sliding tests for 5 % and 10 % WC.

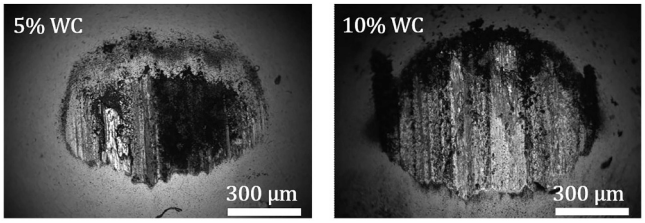

Fig. 23. Worn-out pins corresponding to 5 % and 10 % WC trials.

4. Conclusions

In this work, WC-reinforced Co-base MMC coatings produced by L-DED were analysed. Due to the limited research on the mechanical properties related to strain and flexural behaviour of MMC coatings, not only the hardness and wear resistance but also the bonding strength of Co-WC coatings were investigated. Thus, in order to facilitate the deployment of MMC coatings, comprehensive studies on their flexural behaviour and failure mechanisms need to be carried out.

The mechanical properties of coatings produced by L-DED are highly dependent on the thermal cycle of the manufacturing process. Therefore, coatings produced with different process parameters, preheating conditions, and compositions are tested in the present study. The main contributions of this work are as follows:

(1) The hardness of MMC coatings can be controlled not only by tuning the composition of the feedstock but also by modifying the processing conditions and the thermal cycle. In fact, the microstructure and the subsequent hardness can be effectively controlled through the process parameters.
(2) In contrast, the flexural resistance of MMC coatings remains invariable through the different processing conditions tested. Indeed, all coatings having the same composition exhibited similar results in 3-point bending tests. In sum, the failure of MMC coatings to flexural loads does not depend on the microstructure or properties of the matrix, at least not in a substantial manner.
(3) The composition of the MMC coatings, conversely, does govern the flexural strength of the specimens. Increasing the ceramic content is detrimental to the flexural properties of the coatings, as they exhibit a lower fracture load and deformation. This effect is ascribed to the higher concentration of locally embrittled regions, namely, the reaction layers surrounding the WC particles. Therefore, statistically, more crack initiation sites will be present.
(4) Lastly, a high-quality bond between the substrate and the coating was attained. In fact, after the failure of the sample, the crack propagated through the coating and into the substrate, and no delamination was observed. Therefore, the L-DED process is rendered a suitable alternative to produce high-quality MMC coatings.
(5) A higher wear resistance of the coating containing higher WC% was reported. Indeed, the ceramic particles prevent the metal matrix from wearing off. Neither fractured WC particles nor third-body mechanism was observed. Hence, the tested samples mainly showed a mild abrasive and adhesive wear mechanism, owing to the oxide glaze formed.

It is apparent from the present work that increasing the wear resistance of MMC coatings comes with the cost of decreasing their flexural properties. Varying the processing conditions does not significantly affect the flexural resistance of MMC coatings. Thus, the failure of MMC coatings is ruled almost exclusively by the ceramic phase, and optimisation strategies to enhance the mechanical properties of the matrix do not affect their flexural performance. In short, a balance between the mechanical and wear properties should be sought, relying on the composition of the feedstock as the most relevant factor. In this manner, the composition of MMC coatings could be potentially optimised based on the wear behaviour and the flexural properties; as the wear resistance could be maximised while meeting the requirements in terms of the durability of the coated component.

Funding

This work was supported by the Basque Government (Eusko Jaurlaritza) [grant numbers KK-2022/00070 Edison and KK-2021/00120 Imagine] and the Spanish Ministry of Science and Innovation [grant number PIC2019-109220RB-I00 Alasurf].

CRediT authorship contribution statement

Marta Ostolaza: Conceptualization, Methodology, Investigation, Visualization, Writing – original draft. **Jon Iñaki Arrizubieta:** Conceptualization, Methodology, Investigation, Writing – review & editing, Supervision, Funding acquisition. **Aitzol Lamikiz:** Conceptualization, Methodology, Writing – review & editing, Supervision, Funding acquisition. **Eneko Ukar:** Conceptualization, Writing – review & editing, Supervision, Funding acquisition.

Declaration of competing interest

The authors declare that they have no known competing financial interests or personal relationships that could have appeared to influence the work reported in this paper.

Data availability

Data will be made available on request.

Acknowledgements

Authors would like to acknowledge the Basque Government (Eusko Jaurlaritza) in call IT 1573-22 for the financial support of the research group. In addition, the authors thank for the technical and human support provided by SGIker (UPV/EHU/FEDER, EU), in particular, the Electronic Microscopy and Material Microanalysis Service.

References

[1] X. Ren, H. Zou, Q. Diao, C. Wang, Y. Wang, H. Li, T. Sui, B. Lin, S. Yan, Surface modification technologies for enhancing the tribological properties of cemented carbides: a review, Tribol. Int. 180 (2023), 108257, https://doi.org/10.1016/j.triboint.2023.108257.
[2] L. Zhang, H. Wang, D. Liu, Q. Zhang, W. Guo, N. Yang, J. Xu, S. Fu, B. Yang, S. Liu, S. Zhou, Research on wear detection mechanism of cylinder liner-piston ring based

on energy dissipation and AE, Wear 508–509 (2022), 204472, https://doi.org/10.1016/j.wear.2022.204472.
[3] B. Swain, S. Bhuyan, R. Behera, S.S. Mohapatra, A. Behera, Wear: a serious problem in industry, Tribol. Mater. Manuf. - Wear, Frict. Lubr. (2020), https://doi.org/10.5772/intechopen.94211.
[4] S. Siengchin, A review on lightweight materials for defence applications: a present and future developments, Def. Technol. (2023), https://doi.org/10.1016/j.dt.2023.02.025.
[5] D. Svetlizky, B. Zheng, A. Vyatskikh, M. Das, S. Bose, A. Bandyopadhyay, J. M. Schoenung, E.J. Lavernia, N. Eliaz, Laser-based directed energy deposition (DED-LB) of advanced materials, Mater. Sci. Eng. A 840 (2022), 142967, https://doi.org/10.1016/j.msea.2022.142967.
[6] G. Muvvala, D. Patra Karmakar, A.K. Nath, In-process detection of microstructural changes in laser cladding of in-situ inconel 718/TiC metal matrix composite coating, J. Alloys Compd. 740 (2018) 545–558, https://doi.org/10.1016/j.jallcom.2017.12.364.
[7] S. Zafar, A.K. Sharma, Investigations on flexural performance and residual stresses in nanometric WC-12Co microwave clads, Surf. Coat. Technol. 291 (2016) 413–422, https://doi.org/10.1016/j.surfcoat.2016.03.009.
[8] A.K. Sharma, D. Gupta, On microstructure and flexural strength of metal-ceramic composite cladding developed through microwave heating, Appl. Surf. Sci. 258 (2012) 5583–5592, https://doi.org/10.1016/j.apsusc.2012.02.019.
[9] Y. Li, Y. Xiao, L. Yu, K. Ji, D. Li, A review on the tooling technologies for composites manufacturing of aerospace structures: materials, structures and processes, Compos. Part A Appl. Sci. Manuf. 154 (2022), 106762, https://doi.org/10.1016/j.compositesa.2021.106762.
[10] F. Haftlang, H.S. Kim, A perspective on precipitation-hardening high-entropy alloys fabricated by additive manufacturing, Mater. Des. 211 (2021), 110161, https://doi.org/10.1016/j.matdes.2021.110161.
[11] M. Bhuvanesh Kumar, P. Sathiya, Methods and materials for additive manufacturing: a critical review on advancements and challenges, Thin-Walled Struct. 159 (2021), 107228, https://doi.org/10.1016/j.tws.2020.107228.
[12] T.D. Ngo, A. Kashani, G. Imbalzano, K.T.Q. Nguyen, D. Hui, Additive manufacturing (3D printing): a review of materials, methods, applications and challenges, Compos. Part B Eng. 143 (2018) 172–196, https://doi.org/10.1016/j.compositesb.2018.02.012.
[13] R. Balokhonov, V. Romanova, O. Zinovieva, A. Zemlianov, Microstructure-based analysis of residual stress concentration and plastic strain localization followed by fracture in metal-matrix composites, Eng. Fract. Mech. 259 (2022), 108138, https://doi.org/10.1016/j.engfracmech.2021.108138.
[14] N. Kota, M.S. Charan, T. Laha, S. Roy, Review on development of metal/ceramic interpenetrating phase composites and critical analysis of their properties, Ceram. Int. 48 (2022) 1451–1483, https://doi.org/10.1016/j.ceramint.2021.09.232.
[15] Y. Hu, W. Cong, A review on laser deposition-additive manufacturing of ceramics and ceramic reinforced metal matrix composites, Ceram. Int. 44 (2018) 20599–20612, https://doi.org/10.1016/j.ceramint.2018.08.083.
[16] C. Raahgini, D. Verdi, Abrasive wear performance of laser cladded inconel 625 based metal matrix composites: effect of the vanadium carbide reinforcement phase content, Surf. Coat. Technol. 429 (2022), 127975, https://doi.org/10.1016/j.surfcoat.2021.127975.
[17] N. Li, S. Huang, G. Zhang, R. Qin, W. Liu, H. Xiong, G. Shi, J. Blackburn, Progress in additive manufacturing on new materials: a review, J. Mater. Sci. Technol. 35 (2019) 242–269, https://doi.org/10.1016/j.jmst.2018.09.002.
[18] G. Muvvala, S. Mullick, A.K. Nath, Development of process maps based on molten pool thermal history during laser cladding of inconel 718/TiC metal matrix composite coatings, Surf. Coat. Technol. 399 (2020), https://doi.org/10.1016/j.surfcoat.2020.126100.
[19] J. Li, Z. Zhu, Y. Peng, G. Shen, Phase evolution and wear resistance of in-situ synthesized (Cr, W)23C6-WC composite ceramics reinforced fe-based composite coatings produced by laser cladding, Vacuum 190 (2021), 110242, https://doi.org/10.1016/j.vacuum.2021.110242.
[20] Z. Xie, C. Zhang, R. Wang, D. Li, Y. Zhang, G. Li, X. Lu, Microstructure and wear resistance of WC/Co-based coating on copper by plasma cladding, J. Mater. Res. Technol. 15 (2021) 821–833, https://doi.org/10.1016/j.jmrt.2021.08.114.
[21] S. Zhao, S. Xu, L. Yang, Y. Huang, WC-fe metal-matrix composite coatings fabricated by laser wire cladding, J. Mater. Process. Technol. 301 (2022), 117438, https://doi.org/10.1016/j.jmatprotec.2021.117438.
[22] S. Zhao, C. Jia, Y. Yuan, L. Wang, Y. Huang, L. Yang, Insights into microstructural evolution and dissolution characteristics of reinforced particles in tungsten carbide-nickel composite coatings prepared by laser hot-wire deposition, Int. J. Refract. Met. Hard Mater. 103 (2022), 105720, https://doi.org/10.1016/j.ijrmhm.2021.105720.
[23] G. Muvvala, D. Patra Karmakar, A.K. Nath, Online assessment of TiC decomposition in laser cladding of metal matrix composite coating, Mater. Des. 121 (2017) 310–320, https://doi.org/10.1016/j.matdes.2017.02.061.
[24] K. Deenadayalan, V. Murali, A. Elayaperumal, S. Arulvel, A.Satheesh Kumar, M. Shahedi Asl, Friction and wear properties of short time heat-treated and laser surface re-melted NiCr-WC composite coatings at various dry sliding conditions, J. Mater. Res. Technol. 17 (2022) 3080–3104, https://doi.org/10.1016/j.jmrt.2022.01.124.
[25] J. Yang, F. Liu, X. Miao, F. Yang, Influence of laser cladding process on the magnetic properties of WC-FeNiCr metal-matrix composite coatings, J. Mater. Process. Technol. 212 (2012) 1862–1868, https://doi.org/10.1016/j.jmatprotec.2012.04.009.
[26] R. Liu, J.H. Yao, Q.L. Zhang, M.X. Yao, R. Collier, Sliding wear and solid-particle erosion resistance of a novel high-tungsten stellite alloy, Wear 322–323 (2015) 41–50, https://doi.org/10.1016/j.wear.2014.10.012.
[27] A.I. Mertens, Metal matrix composites processed by laser additive manufacturing: microstructure and properties, in: Addit. Manuf, Elsevier Inc., 2021, pp. 409–425, https://doi.org/10.1016/B978-0-12-818411-0.00005-7.
[28] J. Wang, L. Li, W. Tao, Crack initiation and propagation behavior of WC particles reinforced fe-based metal matrix composite produced by laser melting deposition, Opt. Laser Technol. 82 (2016) 170–182, https://doi.org/10.1016/j.optlastec.2016.03.008.
[29] M. Erfanmanesh, R. Shoja-Razavi, H. Abdollah-Pour, H. Mohammadian-Semnani, M. Barekat, S.H. Hashemi, Friction and wear behavior of laser cladded WC-co and Ni/WC-Co deposits at high temperature, Int. J. Refract. Met. Hard Mater. 81 (2019) 137–148, https://doi.org/10.1016/j.ijrmhm.2019.02.025.
[30] D. Bartkowski, A. Młynarczak, A. Piasecki, B. Dudziak, A. Bartkowska, M. Gościański, Microstructure, microhardness and corrosion resistance of Stellite-6 coatings reinforced with WC particles using laser cladding, Opt. Laser Technol. 68 (2015) 191–201, https://doi.org/10.1016/j.optlastec.2014.12.005.
[31] B. Li, Y. Jin, J. Yao, Z. Li, Q. Zhang, Solid-state fabrication of WCp-reinforced Stellite-6 composite coatings with supersonic laser deposition, Surf. Coat. Technol. 321 (2017) 386–396, https://doi.org/10.1016/j.surfcoat.2017.04.062.
[32] X. Lu, X. Lin, M. Chiumenti, M. Cervera, Y. Hu, X. Ji, L. Ma, H. Yang, W. Huang, Residual stress and distortion of rectangular and S-shaped Ti-6Al-4V parts by directed energy deposition: modelling and experimental calibration, Addit. Manuf. 26 (2019) 166–179, https://doi.org/10.1016/j.addma.2019.02.001.
[33] M. Ostolaza, J.I. Arrizubieta, A. Queguineur, K. Valtonen, A. Lamikiz, I. Flores Ituarte, Influence of process parameters on the particle-matrix interaction of WC-Co metal matrix composites produced by laser-directed energy deposition, Mater. Des. 223 (2022), 111172, https://doi.org/10.1016/j.matdes.2022.111172.
[34] E. Vandersluis, C. Ravindran, Comparison of measurement methods for secondary dendrite arm spacing, Metallogr. Microstruct. Anal. 6 (2017) 89–94, https://doi.org/10.1007/s13632-016-0331-8.
[35] S.J. Wolff, S. Lin, E.J. Faierson, W.K. Liu, G.J. Wagner, J. Cao, A framework to link localized cooling and properties of directed energy deposition (DED)-processed Ti-6Al-4V, Acta Mater. 132 (2017) 106–117, https://doi.org/10.1016/j.actamat.2017.04.027.
[36] C. Guyard, A. Barbangelo, C.H. Allibert, J. Driole, Solidification path and phase equilibria in the liquid-solid range of cobalt-base alloy, J. Mater. Sci. 16 (1981) 604–612, https://doi.org/10.1007/BF02402776.
[37] A. Gholipour, M. Shamanian, F. Ashrafizadeh, Microstructure and wear behavior of stellite 6 cladding on 17–4 PH stainless steel, J. Alloys Compd. 509 (2011) 4905–4909, https://doi.org/10.1016/j.jallcom.2010.09.216.
[38] E.M. Parsons, S.Z. Shaik, Additive manufacturing of aluminum metal matrix composites: mechanical alloying of composite powders and single track consolidation with laser powder bed fusion, Addit. Manuf. 50 (2022), 102450, https://doi.org/10.1016/j.addma.2021.102450.
[39] P.P. Ikubanni, M. Oki, A.A. Adeleke, P.O. Omoniyi, Synthesis, physico-mechanical and microstructural characterization of Al6063/SiC/PKSA hybrid reinforced composites, Sci. Rep. 11 (2021) 1–13, https://doi.org/10.1038/s41598-021-94420-0.